PHILOSOPHICAL TRANSACTIONS A

royalsocietypublishing.org/journal/rsta

Research

Cite this article: Altmeyer SA. 2023 Ferrofluidic wavy Taylor vortices under alternating magnetic field . *Phil. Trans. R. Soc. A* **381**: 20220121.
https://doi.org/10.1098/rsta.2022.0121

Received: 24 July 2022
Accepted: 25 October 2022

One contribution of 12 to a theme issue 'Taylor–Couette and related flows on the centennial of Taylor's seminal *Philosophical Transactions* paper (part 1)'.

Subject Areas:
fluid mechanics, computational physics, computational mechanics, applied mathematics, computational mathematics

Keywords:
Taylor–Couette flow, ferrofluid, alternating magnetic field, resonance phenomena, instability, bifurcations

Author for correspondence:
Sebastian A. Altmeyer
e-mail: sebastian.andreas.altmeyer@upc.edu

Electronic supplementary material is available online at https://doi.org/10.6084/m9.figshare.c.6350552.

THE ROYAL SOCIETY PUBLISHING

Ferrofluidic wavy Taylor vortices under alternating magnetic field

Sebastian A. Altmeyer

Castelldefels School of Telecom and Aerospace Engineering
Universitat Politècnica de Catalunya, Barcelona 08034, Spain

SAA, 0000-0001-5964-0203

Many natural and industrial flows are subject to time-dependent boundary conditions and temporal modulations (e.g. driving frequency), which significantly modify the dynamics compared with their static counterparts. The present problem addresses ferrofluidic wavy vortex flow in Taylor–Couette geometry, with the outer cylinder at rest in a spatially homogeneous magnetic field subject to an alternating modulation. Using a modified Niklas approximation, the effect of frequency modulation on nonlinear flow dynamics and appearing resonance phenomena are investigated in the context of either period doubling or inverse period doubling.

This article is part of the theme issue 'Taylor–Couette and related flows on the centennial of Taylor's seminal *Philosophical Transactions* paper (part 1)'.

1. Introduction

The observation that many flows in nature are driven by periodic forces explains the recent increasing attention given to flow problems which vary periodically in time. One prototypical model system to study such modulated hydrodynamics is the Taylor–Couette system (TCS) [1], which began with the pioneering work of Taylor [2] and has been the subject of intense theoretical and experimental investigations.

Temporal forcing in TCS and resulting effects have been studied in numerous experimental, theoretical and numerical works [3–15]. For example, in the classical Newtonian fluid, the temporal forcing has been imparted to the system in three different ways: first, through harmonically modulated rotations of

© 2023 The Author(s) Published by the Royal Society. All rights reserved.

either the inner or the outer cylinder (or both); second, through harmonic oscillations of the inner cylinder in the axial direction; and third, through pulsation of axially imposed flow or radial throughflow, with the latter requiring porous cylinder walls. The aforementioned means of external forcing have one thing in common: that is, the extra forcing is mechanically introduced into the system via modification of the boundary conditions.

Magnetic fluids, that is, ferrofluids [16], offer an alternative method for realizing such a periodic forcing, which has great advantage for applying direct global modifications into the bulk while the walls remain static. Thus, mechanically, the boundary conditions remain unchanged. Ferrofluids are manufactured fluids consisting of dispersions of magnetized nanoparticles in a variety of liquid carriers [16,17]. Typically, additional surfactant monolayer surrounding the ferromagnetic particles stabilizes the ferrofluid to avoid, or at least minimize, agglomeration effects. In the absence of magnetic field, the magnetic nanoparticles are randomly oriented, and thus, the fluid behaves as a classical fluid with zero net magnetization, and the fluid's viscosity and density typically experience very small alteration due to the presence of the nanoparticles themselves. This situation significantly changes when a magnetic field is present, as, under a sufficiently strong applied magnetic field, the ferrofluid flows towards regions of the magnetic field. As a result, the fluid's properties, such as viscosity, can change. The most prominent example is the magneto-viscous effect [18,19], which significantly changes the hydrodynamics of the system. Applications using ferrofluids are versatile and can be found in various fields and areas, spanning from separation over mechanical positioning to medical applications [20,21] and active flow control [22].

The stability of ferrofluidic Couette flow has been studied in numerous experimental, numerical and theoretical works [16,23–27], with the common observation being that (independent of the field orientation) the basic state becomes stabilized. Singh & Bajaj [28] also investigated numerically the stability of a modulated ferrofluidic Couette flow via parametric excitation of the periodic oscillation in an axially applied (weak) magnetic field. Their findings that variation in frequency and modulation amplitude can either stabilize or destabilize the basic flow, respectively, are in good qualitative agreement with observations in the case of oscillation of the outer cylinder of classical Newtonian fluid [5] .

In this paper, we investigate the problem of active flow control of ferrofluidic Couette flow in the form of variation in the modulation frequency Ω_H of an externally applied alternating magnetic field. Therefore, two different field geometries are discussed. The magnetic field is oriented either *axially* or *transversally*, with the latter breaking the natural system symmetry and rendering all flow states inherently three-dimensional [24,25,29].

Flow structures of particular interest in the present work are wavy Taylor vortex flows (wTVFs) [30–32]. The appearance of such wavy vortices is widely observed in various flow systems, including shear flows, atmospheric flows and rotating convection [33–35]. Most commonly, these wavy states result from a hydrodynamic instability of rotationally invariant basic flow; that is, the flow undergoes a supercritical Hopf bifurcation that breaks the SO(2) symmetry [36–38]. In TCS with only the inner cylinder rotating (outer cylinder at rest), the primary instability consisting of toroidal Taylor vortices (Taylor vortex flow (TVF)) undergoes a second transition while acquiring waviness as the Reynolds number increases. Numerous works have investigated such wavy structures under the aspects of the number of azimuthal waves (wavenumbers), phase speed and variation in rotation direction [30,31,39–44]. A more recent study of the magnetic field-induced flow pattern reversal [22] in wavy vortices illustrated the potential of ferrofluids under the aspect of flow control.

The present work focuses on such wavy structures with small azimuthal wavenumbers, $m=1$ and $m=2$, both azimuthally following the rotation direction like the inner cylinder. We address the question of what happens if an external applied magnetic field is not constant but varies periodically in time with different frequencies. A particular focus lies on resonance phenomena when the modulation frequency reaches multiples or ratios of the natural, that is characteristic, frequency of the studied flow states. The phenomena of both period doubling and inverse period doubling are observed.

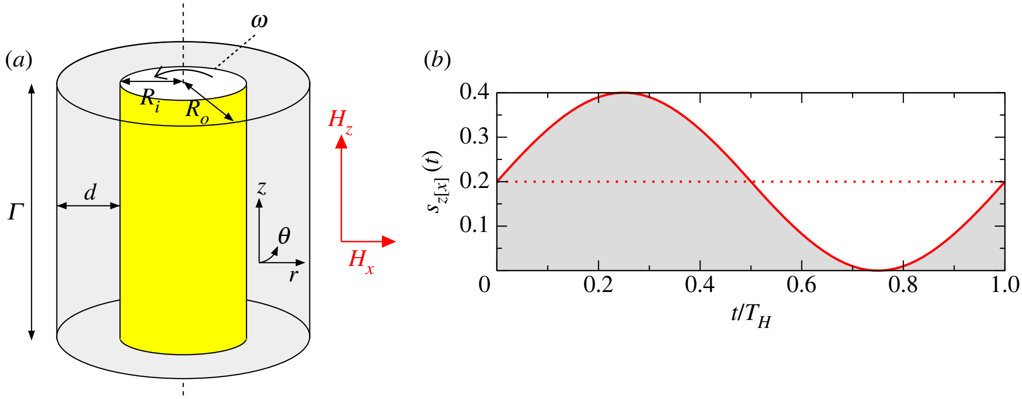

Figure 1. (*a*) Schematic diagram for the TCS with an external applied homogeneous transverse [axial] magnetic field $\mathbf{H}_{ext} = H_x \mathbf{e}_x [H_z \mathbf{e}_z]$. (*b*) Temporal oscillations of the control function $s_{z[x]}(t) = s_{S,z[x]} + s_{M,z[x]} \sin(\Omega_{H_{z[x]}} t)$ over one period. (Online version in colour.)

2. Geometry and system parameters

Flow strength in TCS (figure 1(*a*)) is commonly represented in terms of the Reynolds number $Re = \omega R_i d/\nu$, which characterizes the ratio between inertia and viscous forces and has been proven to be a well-suited parameter to describe the driving of the system [32]. Here, R_i is the radius of the inner cylinder, and ω is the angular velocity of the inner cylinder. Periodic boundary conditions are imposed in the axial (z) direction, with imposed wavenumber $k = \pi$ and no-slip boundary conditions on the cylinder surfaces. The cylindrical coordinate system (r, θ, z) by the velocity field $\mathbf{u} = (u, v, w)$ and the corresponding vorticity field $\nabla \times \mathbf{u} = (\xi, \eta, \zeta)$ can be used to describe the system. In this work, the radius ratio of the cylinders is kept fixed at 0.8 and the inner cylinder is considered to rotate with $Re = 140$ while the outer cylinder is at rest. The time and length scales are made dimensionless by diffusion time d^2/ν and gap width d, and the pressure in the fluid is normalized by $\rho\nu^2/d^2$.

To realize a periodically modulated TCS, we apply a sinusoidal modulation signal (figure 1(*b*)) to the external magnetic field, which is oriented either parallel (z) or transverse (perpendicular) (x) to the system symmetry axis. The fields are further assumed to be uniform in space and harmonic in time, that is, $\mathbf{H}_{z[x]} = [H_{S,z[x]} + H_{M,z[x]} \sin(\Omega_{H_{z[x]}} t)]\mathbf{e}_z[\mathbf{e}_x]$. It is important to mention that a pure axially oriented magnetic field does *not* change the system symmetry, while a pure transversally oriented magnetic field does and renders all flow states inherently three-dimensional [24]. Thus, strictly speaking, the 'pure' classical structures do not exist anymore; instead, only solutions modulated with the $m = 2$ mode are present, that is CCF_2 and TVF_2 [45–47]. For both field configurations, the stability thresholds are shifted to larger control parameters, which means a stabilizing effect on the basic state, as previously reported in different experimental and numerical works [24,25,29,46].

The magnetic field **H** and the magnetization **M** are conveniently normalized by the quantity $\sqrt{\rho/\mu_0}\nu/d$, with free space permeability μ_0. By using a modified Niklas approach [23,24,48,49], the effect of the magnetic field and the magnetic properties of the ferrofluid on the velocity field can be characterized by a single (time-dependent) function,

$$s_{z[x]}(t) = s_{S,z[x]} + s_{M,z[x]} \sin(\Omega_{H_{z[x]}} t), \tag{2.1}$$

with $s_{S,z[x]}$ being the static contribution of the driving, $s_{M,z[x]}$ the modulation amplitude and $\Omega_{H_{z,[x]}}$ the modulation frequency, respectively. See appendix A for further details.

3. Methods

(a) Direct numerical simulations

Direct numerical simulations (DNS) for ferrohydrodynamical flow using the Niklas approximation are employed [23,24]. In the present study, we consider periodic boundary conditions in the axial direction corresponding to a fixed axial wavenumber, $k = \pi$ ($\lambda = 2$), motivated by various experimental findings for the appearance of primary TVF instability in the Taylor–Couette flow, with the outer cylinder at rest [1,30–32]. No-slip boundary conditions are used on the cylinder surfaces, and the radius ratio of inner and outer cylinders is kept fixed at $R_i/R_o = 0.8$. The DNS are conducted by combining a standard, second-order finite-difference scheme in (r, z) with a Fourier spectral decomposition in θ and an explicit time splitting. The outer cylinder is at rest while the inner one is rotating with a fixed Reynolds number of $Re = 140$ and an explored parameter range spanning $0 \leq (s_{z[x],S}, s_{z[x],M}) \leq 1$, and $0 \leq \Omega_H \leq 10^3$.

(b) Ferrohydrodynamical equation of motion

The non-dimensionalized hydrodynamical equations [29,50,51] are derived from

$$(\partial_t + \mathbf{u} \cdot \nabla)\mathbf{u} - \nabla^2 \mathbf{u} + \nabla p = (\mathbf{M} \cdot \nabla)\mathbf{H} + \frac{1}{2} \nabla \times (\mathbf{M} \times \mathbf{H}),$$

$$\nabla \cdot \mathbf{u} = 0. \tag{3.1}$$

The velocity fields on the cylindrical surfaces are $\mathbf{u}(r_i, \theta, z) = (0, Re, 0)$ and $\mathbf{u}(r_o, \theta, z) = (0, 0, 0)$, where the non-dimensional inner and outer radii are $r_i = R_i/(R_o - R_i)$ and $r_o = R_o/(R_o - R_i)$, respectively.

Equation (3.1) is solved with an equation describing the magnetization of the ferrofluid. Here, we consider an equilibrium magnetization of an unperturbed state with homogeneously magnetized ferrofluid at rest. Thereby the mean magnetic moment is oriented (aligned) in the direction of the magnetic field: $\mathbf{M}^{\mathrm{eq}} = \chi \mathbf{H}$. Langevin's formula [52] is used to approximate the ferrofluid's magnetic susceptibility χ. The initial value χ is set to 0.9 with the use of a linear magnetization law. Here, we consider the ferrofluid APG933 [53].[1] The near-equilibrium approximation by Niklas [23,27] assumes small derivations $||\mathbf{M} - \mathbf{M}^{\mathrm{eq}}||$ and small magnetic relaxation time τ: $|\nabla \times \mathbf{u}|\tau \ll 1$. Using these approximations, the following magnetization equation can be obtained [51]:

$$\mathbf{M} - \mathbf{M}^{\mathrm{eq}} = c_N^2 \left(\frac{1}{2} \nabla \times \mathbf{u} \times \mathbf{H} + \lambda_2 \mathbb{S}\mathbf{H} \right), \tag{3.2}$$

where

$$c_N^2 = \tau/(1/\chi + \tau\mu_0 H^2/6\mu\Phi) \tag{3.3}$$

is the Niklas coefficient [23], μ is the dynamic viscosity, Φ is the volume fraction of the magnetic material, $\mathbb{S}$ is the symmetric component of the velocity gradient tensor [50,51] and λ_2 is the material-dependent transport coefficient [50], which we choose to be $\lambda_2 = 4/5$ [50,51,54]. Using (3.2), the magnetization in (3.1) can be eliminated to obtain the following ferrohydrodynamical equation of motion [29,48–51]:

$$(\partial_t + \mathbf{u} \cdot \nabla)\mathbf{u} - \nabla^2 \mathbf{u} + \nabla p_M = -\frac{s_N^2}{2} \left[\mathbf{H} \nabla \cdot \left(\mathbf{F} + \frac{4}{5} \mathbb{S}\mathbf{H} \right) + \mathbf{H} \times \nabla \times \left(\mathbf{F} + \frac{4}{5} \mathbb{S}\mathbf{H} \right) \right], \tag{3.4}$$

where $\mathbf{F} = (\nabla \times \mathbf{u}/2) \times \mathbf{H}$, p_M is the dynamic pressure incorporating all magnetic terms that can be expressed as gradients, and s_z is the Niklas function (the classical static Niklas parameter; see (A1)). To the leading order, the internal magnetic field in the ferrofluid can be approximated

[1] The specifications for the ferrofluid APG933 are as follows: $\mu_0 M_s = 20\,\mathrm{mT}$, $\eta = 500\,\mathrm{mPas}$, density $\rho = 1.09\,\mathrm{g\,cm^{-3}}$, $\Phi_m = 3.3\%$, susceptibility $\chi = 0.9$, mean diameter of the particle's magnetic core 10 nm, thickness of the polymeric coating 2 nm.

as the externally imposed field [29], which is reasonable for obtaining dynamic solutions of the magnetically driven fluid motion. Further simplification of (3.4) leads to

$$(\partial_t + \mathbf{u}\cdot\nabla)\mathbf{u} - \nabla^2\mathbf{u} + \nabla p_M = s_N^2 \left\{ \nabla^2\mathbf{u} - \frac{4}{5}[\nabla\cdot(\mathbb{S}\mathbf{H})] \right.$$
$$\left. -\mathbf{H}\times\left[\frac{1}{2}\nabla\times(\nabla\times\mathbf{u}\times\mathbf{H}) - \mathbf{H}\times(\nabla^2\mathbf{u}) + \frac{4}{5}\nabla\times(\mathbb{S}\mathbf{H})\right]\right\}. \tag{3.5}$$

For more detailed descriptions of these hydrodynamical equations and how to derive the Niklas function, see appendix A.

(c) Numerics

The ferrohydrodynamical equations of motion (3.4) are solved [23,24,29,51,55] using a standard, second-order finite-difference scheme in (r,z), combined with a Fourier spectral decomposition in θ and (explicit) time splitting. The variables in the finite-difference scheme in (r,z) can be expressed as

$$f(r,\theta,z,t) = \sum_{m=-m_{\max}}^{m_{\max}} f_m(r,z,t)\,\mathrm{e}^{im\theta}, \tag{3.6}$$

where f denotes one of the variables $\{u,v,w,p\}$. For the parameter regimes considered, the choice $m_{\max}=16$ provides adequate accuracy. Explicit time splitting is used. For the explored parameter space, the choice of 16 azimuthal modes provides adequate accuracy. Uniform grids with spacing $\delta r=\delta z=0.02$ and time steps $\delta t<1/3800$ are used. For diagnostic purposes, we also evaluate the complex mode amplitudes $f_{m,n}(r,t)$ obtained from a Fourier decomposition in the axial direction:

$$f_m(r,z,t) = \sum_n f_{m,n}(r,t)\,\mathrm{e}^{inkz}, \tag{3.7}$$

where $k=2\pi d/\lambda$ is the axial wavenumber.

4. Results

Before discussing the effect of an alternating magnetic field, it is important to recall the main observations for ferrofluids under static applied magnetic fields. A pure axially oriented magnetic field leaves the flow structure unchanged and only alters the bifurcation and stability threshold. By contrast, a magnetic field with a finite transverse component modifies classical system symmetries, and as a result, the flow structures become inherently three-dimensional [24,25,29]. To be more precise, the azimuthal mode $m=2$ becomes stimulated and finite in the presence of such a transverse field [24], physically originating from the fact that the magnetic field enters the annulus on one side and exits on the opposite side. Following our earlier introduced notation [46,47], these modified solutions are identified with the index $_2$.

(a) Static scenario

For the given set of parameters, one finds two wavy states coexisting, 1-wTVF$_{[2]}$ and 2-wTVF$_{[2]}$, which are distinguished by their azimuthal wavenumber m. Both solutions bifurcate from the primary TVF$_{[2]}$ at a lower Re, while 1-wTVF$_{[2]}$ stably. By contrast, 2-wTVF$_{[2]}$ appears out of the unstable TVF$_{[2]}$ branch and becomes stabilized with increasing Re. In any case, the studied parameters are chosen to be sufficiently far away from any critical points to guarantee that the solutions remain supercritical and stable for oscillating fields as well.

(b) Flow structures and dynamics

Figure 2 presents different flow visualizations of 1-wTVF$_{[2]}$ and 2-wTVF$_{[2]}$ at $Re=140$ in the absence of any magnetic field, as within a static axial and transverse field, respectively. Obviously,

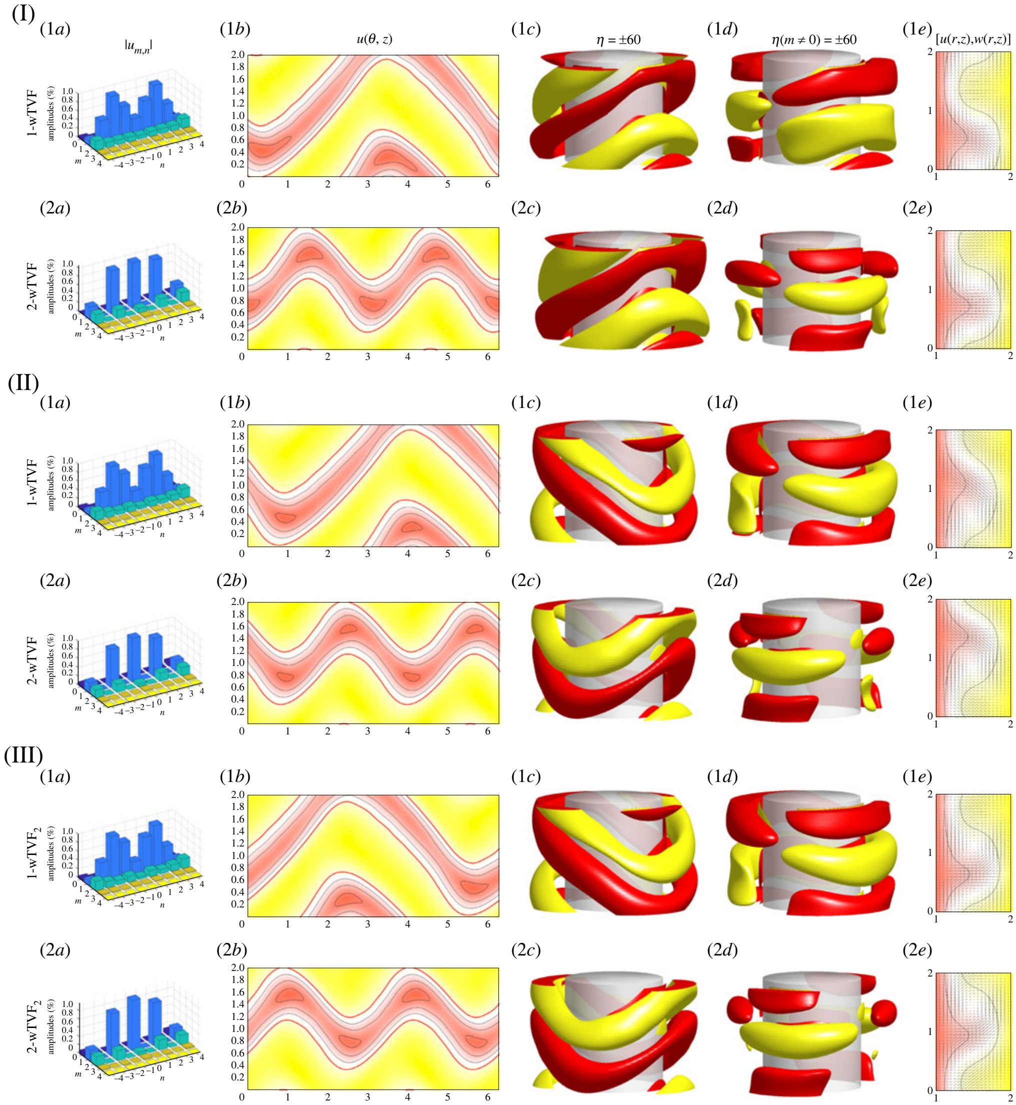

Figure 2. Flow visualization of different stable flow structures for $Re = 140$: (I) without magnetic field $s_{x,z}(t) = 0$, (II) pure axial (static) magnetic field $(s_{S,z}) = 0.2$ and (III) pure transverse (static) magnetic field $(s_{S,x}) = 0.2$. Snapshots of (1) 1-wTVF$_{[2]}$, (2) 2-wTVF$_{[2]}$. Shown are (*a*) Fourier spectrum (m, n) (scaled with max = 1), (*b*) the radial velocity $u(\theta, z)$ on an unrolled cylindrical surface in the annulus at mid-gap (red [dark gray] (yellow [light gray]) colour indicates in (out) flow), isosurfaces of (*c*) η for full structure and (*d*) $\eta(\neq 0)$ without the symmetric subspace $m = 0$ (red [dark grey] and yellow [light grey] colours correspond to positive and negative values, respectively, with zero specified as white) and (*e*) vector plot $[u(r,z), w(r,z)]$ (at $\theta = 0$) of the radial and axial velocity components (including the colour-coded azimuthal velocity v). (Online version in colour.)

both flow states consist of helical closed vortices (figure 2(*b*,*c*)) and therefore have $m = 0$ as the dominant azimuthal wavenumber. However, the Fourier spectrum (m, n) (figure 2(*a*)) highlights the second dominant azimuthal wavenumber as different: $m = 1$ for 1-wTVF$_{[2]}$ and $m = 2$ for 2-wTVF$_{[2]}$. As a result, one or two wobble(s), respectively, can be observed in the azimuthal direction once surrounding the annulus. Although 1-wTVF$_{[2]}$ includes the $m = 2$ mode as a higher harmonic, a characteristic feature for 2-wTVF$_{[2]}$ is the absence (without any field) or minority of the $m = 1$ mode (figure 2(2*a*)). The additional $m = \pm 2$ modes' stimulation forced by the transverse magnetic field [24,25] is the most visible in the contours of the radial velocity $u(\theta, z)$ for 2-wTVF$_2$

(figure 2(2*b*)). The contours narrow and expand, respectively, with a period π (e.g. see the different sizes in the contours of the small islands). Snapshots in figure 2(*d*) show the contribution of all but the azimuthal dominant mode $m = 0$.

The wTVF flows have a characteristic period that depends on various system parameters. The presence of a static magnetic field only has a minor effect on these periods. For the given parameters, we observed the following periods: in the absence of any field: $\tau_{1\text{-wTVF}} = 0.417$ and $\tau_{2\text{-wTVF}} = 0.214$, for an axial field, $\tau_{1\text{-wTVF}} = 0.424$ and $\tau_{2\text{-wTVF}} = 0.217$ and for a transverse field, $\tau_{1\text{-wTVF}_2} = 0.419$ and $\tau_{2\text{-wTVF}_2} = 0.213$. Thus, the effect for static magnetic fields can be ignored.

(c) Oscillating fields

Figure 3 illustrates the time series of the radial flow field modes $|u_{0,1}|$ and $|u_{2,1}|$ for 1-wTVF$_{[2]}$ and 2-wTVF$_{[2]}$ under axial and transverse oscillating fields. The two modes $|u_{0,1}|$ and $|u_{2,1}|$ are chosen, as they are present in both flow structures 1-wTVF$_{[2]}$ and 2-wTVF$_{[2]}$, with $m = 0$ in general being the dominant one highlighting the azimuthal closed vortex structure. Presented frequencies Ω_H are integer multiples and/or ratios of the characteristic frequencies for 1-wTVF ($\Omega_H = 15$) and 2-wTVF ($\Omega_H = 30$) in the absence of any oscillation together with the high-frequency limit $\Omega_H = 100$ [48]. A common observation is that in the high-frequency limit Ω_H, the amplitude variation becomes smaller and only the average of the oscillating field plays a role [48,55]. Apart from the average mode, amplitudes in the high-frequency limit are smaller than those for the corresponding static case, which is an indication that the oscillating field moves the wavy states closer to its bifurcation onset for both axial and transverse fields. However, there is at least one significant difference between axial and transverse oscillating fields. In the case of symmetry breaking transverse fields, further subharmonic resonances appear as nonlinear superpositions of oscillation frequency Ω_H and the natural system frequencies. The result is visible in the appearance of long periods (figure 3(II)) and the corresponding observation of low frequencies f_{LF} (see also figure 7(*a*)).

Figure 4 shows the dominant mode amplitude $|u_{0,1}|$ as a function of the reduced time $t/\tau_{1[2]\text{-wTVF}_{[2]}}$ concerning the corresponding wavy vortex solution. In the absence of any magnetic field and for a static applied (axial and transverse) magnetic field, the mode amplitude $|u_{0,1}|$ shows one and two periodic oscillations over one period for 2-wTVF$_{[2]}$ and 1-wTVF$_{[2]}$, respectively. This also highlights the fact that the period relations are almost $2 \times \tau_{2\text{-wTVF}_{[2]}} \approx \tau_{1\text{-wTVF}_{[2]}}$. For comparison, the high-frequency limit $\Omega_H = 100$ is also shown. There is obviously no resonance, as there is no integer multiple that fits in the periods of the wavy solutions.

When the external driving frequency Ω_H (period τ_H) is an integer multiple (or fraction, that is half) of the natural frequency of the wavy solution, resonances appear at $\Omega_H = 15, 30$ and 60. Note the period doubling at $\Omega_H = 15$ for 2-wTVF$_{[2]}$ which results in the fact that only a single oscillation is visible in the scaled mode amplitude (figure 4), although based on the fact that $\Omega_H = 15$ is just about half of the natural frequency of 2-wTVF$_{[1]}$. (For visualization of the corresponding periods, see also figure 8).

Additionally, for the lower frequencies $\Omega_H = 15$ and 30, one sees an asymmetry in the amplitude of the radial flow field mode $|u_{0,1}|$ caused by the nonlinear increase in the stability of the bifurcation thresholds of the wavy structures.

(d) Phase space evolution

With variation in the driving frequency Ω_H, the phase space explored by the trajectories of the corresponding wavy solutions is altered and expanded. Figure 5 presents this phase space for 1-wTVF$_{[2]}$ and 2-wTVF$_{[2]}$ under axial and transverse magnetic fields and driving frequencies, as indicated.

For static (axially or transversally oriented) magnetic fields, the flow characteristics remain unchanged compared to the situation in the absence of any magnetic field. TVF and TVF$_2$ remain fixed-point (fp) solutions and 1-wTVF$_{[2]}$ and 2-wTVF$_{[2]}$ remain limit cycles (lc) (figure 5(1,2*a*,3*a*)).

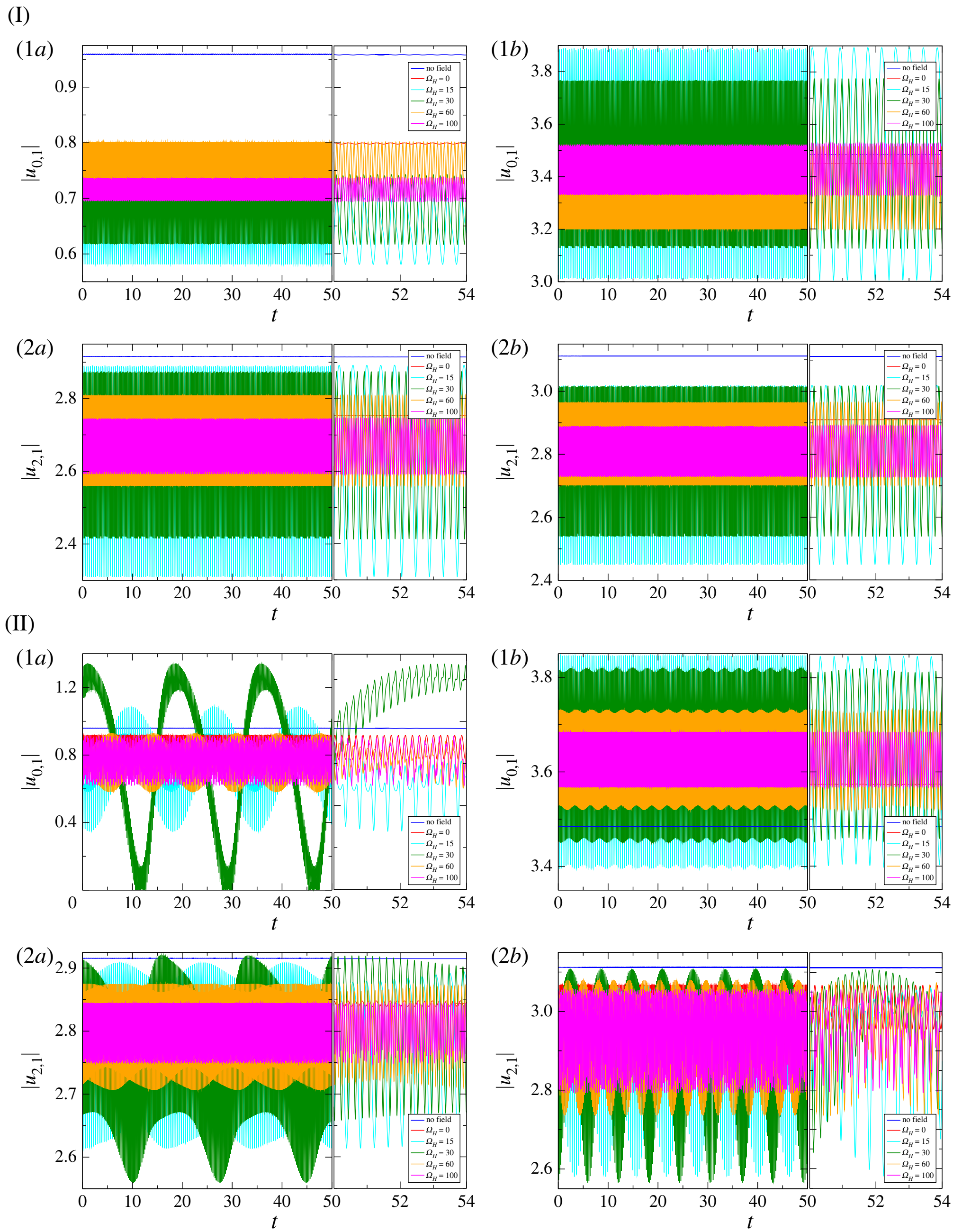

Figure 3. Time series of radial flow field modes (1) $|u_{0,1}|$ and (2) $|u_{2,1}|$ for (*a*) 1-wTVF$_{[2]}$ and (*b*) 2-wTVF$_{[2]}$ under (I) axial magnetic field $s_{z,S} = 0.2$, $s_{z,M} = 0.2$ and (II) transverse magnetic field $s_{x,S} = 0.2$, $s_{x,M} = 0.2$ for different frequencies Ω_H as indicated. (Online version in colour.)

With an alternating magnetic field, the flow dynamics become more complex. To be precise, the complexity increases by one order. Due to the added time dependence, TVF and TVF$_2$ change from fp to lc, while 1-wTVF$_{[2]}$ and 2-wTVF$_{[2]}$ change from lc to quasi-periodic (qp) solutions living on a 2-torus (T2). The latter is visible in the observation of closed cycles within the Poincaré sections (E_{kin}, η_+) for $\eta_- = 0$ (insets in figure 5).

royalsocietypublishing.org/journal/rsta *Phil. Trans. R. Soc. A* **381**: 20220121

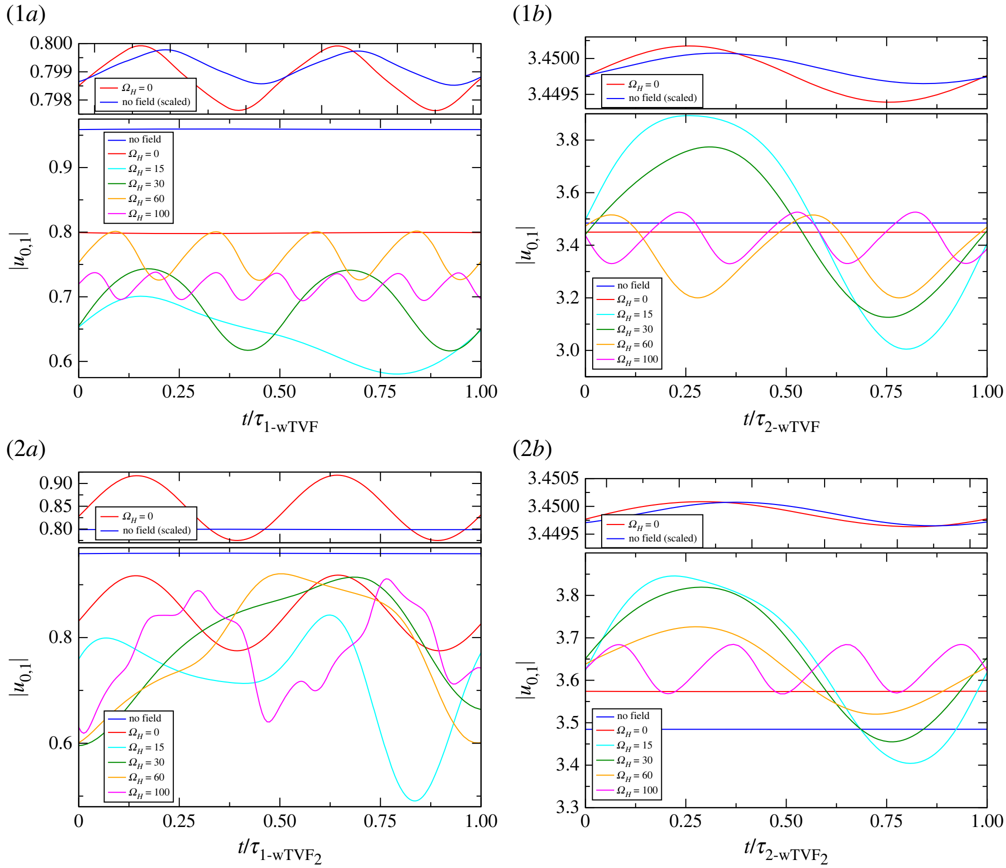

Figure 4. The dominant mode amplitude $|u_{0,1}|$ as a function of the reduced time $t/\tau_{1[2]\text{-wTVF}_{[2]}}$ for (*a*) 1-wTVF$_{[2]}$ and (*b*) 2-wTVF$_{[2]}$ under (1) axial and (2) transverse magnetic field at modulation frequencies as indicated. For visibility and comparability reasons the 'no-field' curves (in the upper part of each graphics) have been scaled to the mean value of the corresponding curves for static fields but in the absence of any oscillation ($\Omega_H = 0$) (cf. figure 3). (Online version in colour.)

With the alternating magnetic field, the trajectories of both qp solutions (1-wTVF$_{[2]}$ and 2-wTVF$_{[2]}$) explore wider areas within the parameter space (η_+, η_-). This effect is most pronounced and visible at small driving frequencies Ω_H, and the phase space area becomes narrower with increasing Ω_H, consistent with the shrinking of the mode amplitudes for larger Ω_H (cf. figure 3).

However, even though the flow structures increase one order in complexity when an alternating field is present (fp to lc and lc to qp), their flow characteristics and dynamics remain unchanged. When Ω_H increases, a first resonance appears for the driving frequency $\Omega_H = 15$, which is equal (in fact it is only very close to be precise) to the 'natural' frequency for 1-wTVF$_{[2]}$, resulting in additional forcing of this solution. Meanwhile, the effect on 2-wTVF$_{[2]}$ is much more prominent. As $\Omega_H = 15$ is about half the natural frequency for 2-wTVF$_{[2]}$ ($\Omega_H = 30$), *period doubling* can be clearly visible in the Poincaré sections (E_{kin}, η_+) in figure 5(2*b*,3*b*) (for a transverse field this is not so visible due to the additional $m = 2$ modes). For larger Ω_H, after the resonance, the Poincaré sections again illustrate a single circle (figure 5(*c*,*d*)). An alternating field with the driving frequency $\Omega_H = 30$ forces the natural frequency of 2-wTVF$_{[2]}$. Meanwhile, $\Omega_H = 30$ is just double the natural frequency (half of the period) of 1-wTVF$_{[2]}$, and one sees a resonance with modified dynamics in half the natural period. In some way, this is like an *inverse period doubling* [56,57], although here it only appears at discrete frequency Ω_H and afterwards disappears again.

royalsocietypublishing.org/journal/rsta Phil. Trans. R. Soc. A 381: 20220121

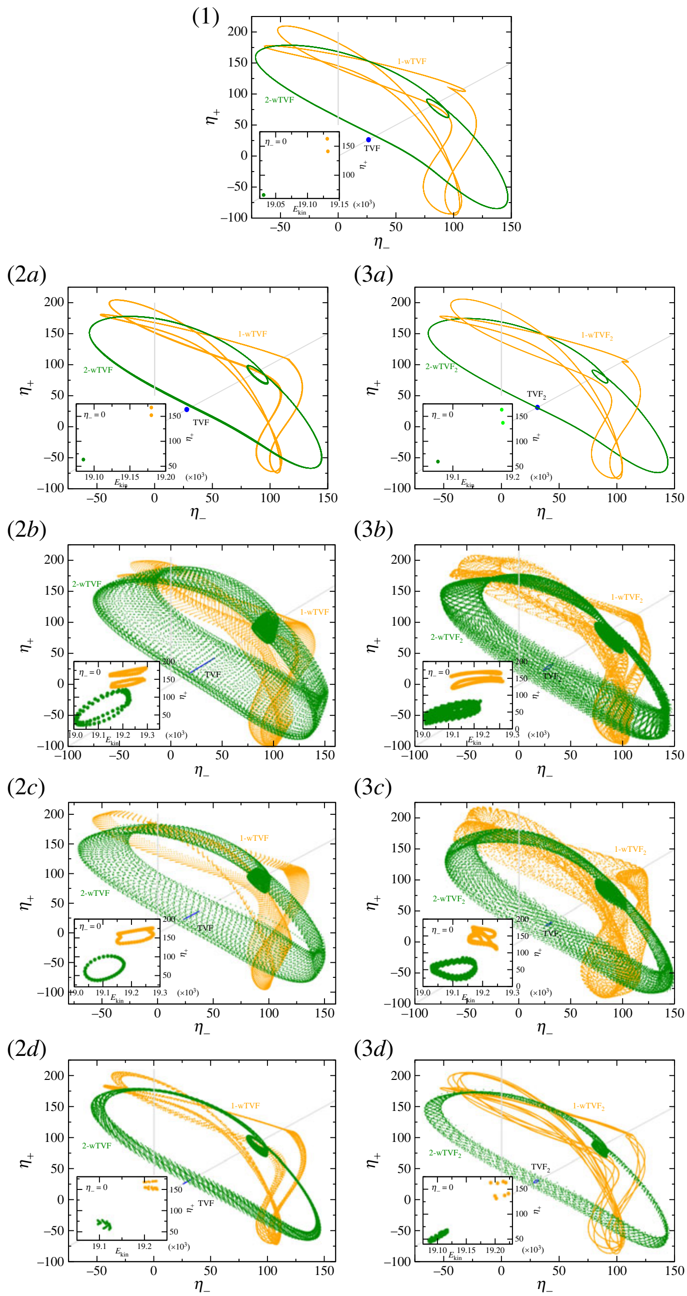

Figure 5. Phase portraits of 1-wTVF$_{[2]}$ and 2-wTVF$_{[2]}$ for (1) no field $s(t) = 0$, (2) $s_{z,S} = 0.2$, $s_{z,M} = 0.2$ axial magnetic field and (3) $s_{x,S} = 0.2$, $s_{x,M} = 0.2$ transverse magnetic field for different modulation frequencies (*a*) $\Omega_H = 0$, (*b*) $\Omega_H = 15$, (*c*) $\Omega_H = 30$ and (*d*) $\Omega_H = 100$ on $(\eta_-, \eta_+) = (\eta(r = d/2, \theta = 0, z = \Gamma/4), \eta(r = d/2, \theta = 0, z = 3\Gamma/4))$. Insets show corresponding two-dimensional Poincaré sections $(E_{\rm kin}, \eta_+)$ for $\eta_- = 0$ (highlighted by vertical grey line). Due to symmetry reasons, the limit cycle solutions for TVF under the axial field (2*b*, 2*c*, 2*d*) and projection in (η_-, η_+) appear as a single line (degenerated solution) on the diagonal line $\eta_- = \eta_+$, while under the transverse field (3*b*, 3*c*, 3*d*) the limit cycle is visible for the modified TVF$_2$. (Online version in colour.)

The next resonance appears at $\Omega_H = 60$, which is twice and four times the natural frequency of 2-wTVF$_{[2]}$ and 1-wTVF$_{[2]}$, respectively. When the alternating frequency Ω_H is further increased, higher oscillations appear on top of the main flow dynamics characterizing the wavy solutions, together with decreasing amplitudes. As described before, the time series of mode amplitudes and the parameter region explored by the trajectories of the wavy solutions shrink together.

Due to symmetry reasons, the limit cycle solutions for TVF under the alternating axial field (figure 5(2*b*,*c*,*d*)) appear in the projection in (η_-, η_+) as a single line (degenerated solution) on the diagonal line $\eta_- = \eta_+$, while for the alternating transverse field, the limit cycle of modified TVF_2 is visible (figure 5(3*b*,3*c*)).

(e) Resonances

To gain a more quantitative insight into the effect that the oscillating fields have on the different flow states, figures 6 and 7 present power spectral densities (PSDs) and time series (insets) of the dominant radial flow field mode $|u_{0,1}|$.

For static magnetic fields, either axial or transversal, the time series of $|u_{0,1}|$ remains qualitatively the same as in the absence of any magnetic field; solely a larger amplitude can be seen under transverse field (figure 3(II)). In any case, the corresponding PSDs and time series $|u_{0,1}|$ for both 1-wTVF$_{[2]}$ and 2-wTVF$_{[2]}$, respectively, illustrate the dynamics associated with one single frequency f (or corresponding period τ, cf. inset in figures 6(1) and 7(1)), giving the flows to have a limited cycle solution.

With the appearance of the first resonance at $\Omega_H = 15$, the PSDs for 1-wTVF$_{[2]}$ in figures 6(2*a*) and 7(2*a*) remain qualitatively unchanged, illustrating a driving with its own natural frequency. Meanwhile, the PSDs for 2-wTVF$_{[2]}$ in figures 6(2*b*) and 7(2*b*) show the appearance of a new frequency, that is, the driving frequency f_H, which is just half of the natural frequency. The double period is visible in the insets (cf. Poincaré sections in figure 5).

At the second resonance $\Omega_H = 30$, the PSDs for 2-wTVF$_{[2]}$ in figures 6(3*a*) and 7(3*a*) remain qualitatively unchanged compared to the one in the absence of any oscillation due to forcing with its natural frequency. By contrast, this driving frequency is now just double the natural frequency for 1-wTVF$_{[2]}$ (figures 6(3*a*) and 7(3*a*)). As a result, the corresponding period is reduced to half its original time (see insets), that is, an inverse period doubling.

For alternating axially oriented fields the PSDs in the high-frequency limit ($\Omega_H = 100$) in figure 6(4*a*,4*b*) illustrate that the additionally introduced frequency only results in modulation on top of the main frequency of the wavy solutions. This also mainly holds for the wavy solutions under alternating transverse fields, with the interesting fact that the double of the main frequency (half of the period) is most pronounced (figure 7(4*a*,4*b*)).

It is worth mentioning that such simplification in flow dynamics due to external forcing has been detected in other systems. For example, Sarwar *et al.* [57] described the physical mechanism of inverse period doubling cascade in a study of the flow past a circular cylinder forced by a fluidic actuation and the resulting transition from a mildly chaotic to perfectly periodic state for quasi-statically increased forcing amplitude.

(f) Low-frequency modulations

A crucial difference between the two different field orientations is the fact that for an alternating transverse magnetic field an additional *long period modulation* τ_{LF} (low frequency) appears (figure 3(II)). Thus, in the corresponding PSDs a low frequency f_{LF} can be detected. In general, the PSDs for an alternating transverse magnetic field are more complex because any transverse field breaks the classical system symmetries and introduces $m = \pm 2$ mode components.

Figure 8 provides an overview of the different stimulated frequencies with variations in the alternating frequency Ω_H (I) together with variations of the corresponding periods τ (II). The actual period τ of the wavy states is highlighted by large squares (for better visibility connected by dashed lines), while other linear and nonlinear triggered periods are shown as indicated in the caption. Small arrows below indicate the different resonance scenarios at $\Omega_H = 15, 30, 60$ and 90. Thereby, resonance for $\Omega_H = 90$ is only found in transverse magnetic fields.

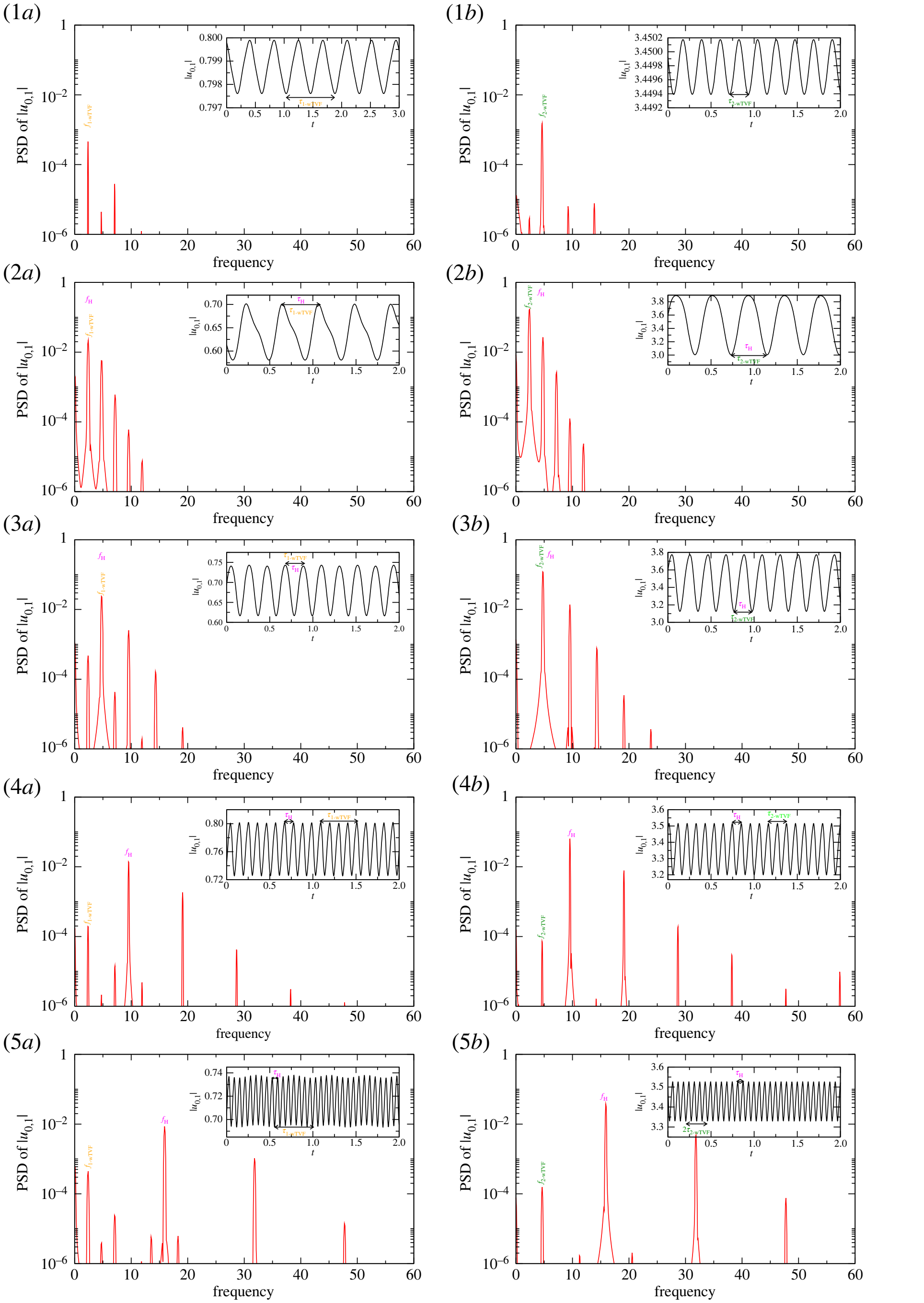

Figure 6. Power spectral densities (PSDs) and time series (insets) of the dominant radial flow field mode $|u_{0,1}|$ for (*a*) 1-wTVF and (*b*) 2-wTVF and variation in Ω_H. (1) $\Omega_H = 0 : \tau_{1\text{-wTVF}} = 0.4238$; $\tau_{2\text{-wTVF}} = 0.2173$, (2) $\Omega_H = 15 : \tau_{1\text{-wTVF}} = 0.4149$; $\tau_{2\text{-wTVF}} = 0.4076$, (3) $\Omega_H = 30 : \tau_{1\text{-wTVF}} = 0.4224$; $\tau_{2\text{-wTVF}} = 0.2110$, (4) $\Omega_H = 60 : \tau_{1\text{-wTVF}} = 0.4171$; $\tau_{2\text{-wTVF}} = 0.2137$, (5) $\Omega_H = 100 : \tau_{1\text{-wTVF}} = 0.4207$; $\tau_{2\text{-wTVF}} = 0.2139$. Field parameters: $s_{z,S} = 0.2$, $s_{z,M} = 0.2$. Note that in the pure axial field, no low frequency (f_{LF}) is found. (Online version in colour.)

The fact that under a transverse magnetic field the flow is inherently three-dimensional due to $m = 2$ mode stimulation results in a more complex scenario. The azimuthal rotating wavy states have to pass through these localized fixed $m = 2$ belly vortices generated at the opposite

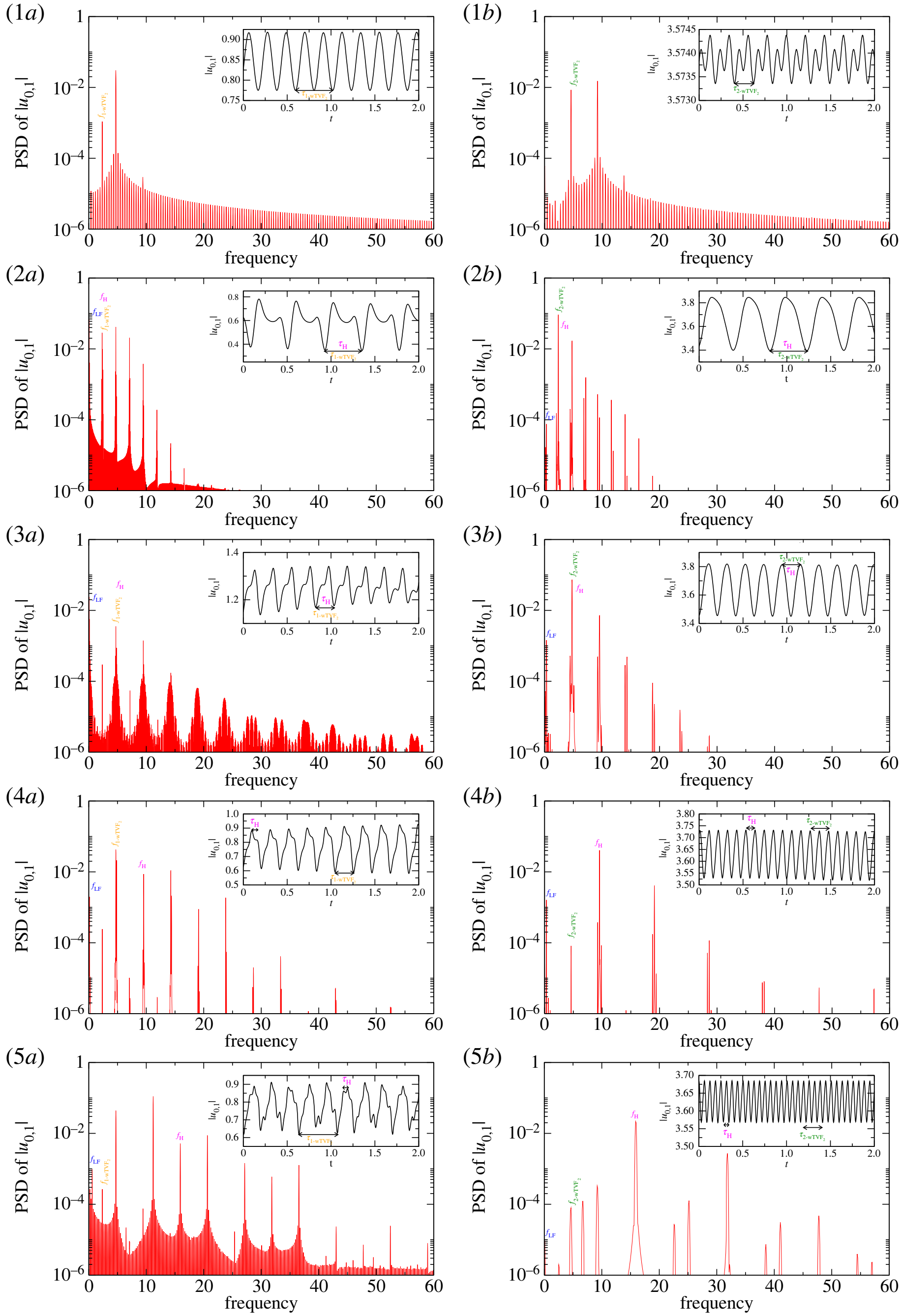

Figure 7. (See also figure 6) Power spectral densities (PSDs) and time series (insets) of the dominant radial flow field mode $|u_{0,1}|$ for (*a*) 1-wTVF$_2$ and (*b*) 2-wTVF$_2$ and variation in Ω_H. (1) $\Omega_H = 0$: $\tau_{1\text{-wTVF}_2} = 0.4141$; $\tau_{2\text{-wTVF}_2} = 0.2134$, (2) $\Omega_H = 15$: $\tau_{1\text{-wTVF}_2} = 0.4210$; $\tau_{\mathrm{LF}} = 15.873$ $\tau_{2\text{-wTVF}_2} = 0.4163$; $\tau_{\mathrm{LF}} = 2.4286$, (3) $\Omega_H = 30$: $\tau_{1\text{-wTVF}_2} = 0.2081$; $\tau_{\mathrm{LF}} = 16.528$ $\tau_{2\text{-wTVF}_2} = 0.2059$; $\tau_{\mathrm{LF}} = 3.0454$, (4) $\Omega_H = 60$: $\tau_{1\text{-wTVF}_2} = 0.2073$; $\tau_{\mathrm{LF}} = 5.2307$; $\tau_{2\text{-wTVF}_2} = 0.2172$; $\tau_{\mathrm{LF}} = 2.956$ and (5) $\Omega_H = 100$: $\tau_{1\text{-wTVF}_2} = 0.4175$; $\tau_{2\text{-wTVF}_2} = 0.2152$; $\tau_{\mathrm{LF}} = 10.258$. Field parameters: $s_{x,S} = 0.2$, $x_{z,M} = 0.2$. (Online version in colour.)

position where the field enters and exits the annulus, respectively [24,29]. As a result, many more modes become finite, and therefore, the corresponding PSDs are more complex, with the general observation of a single low-frequency f_{LF}, which is absent for axial magnetic fields (figure 8).

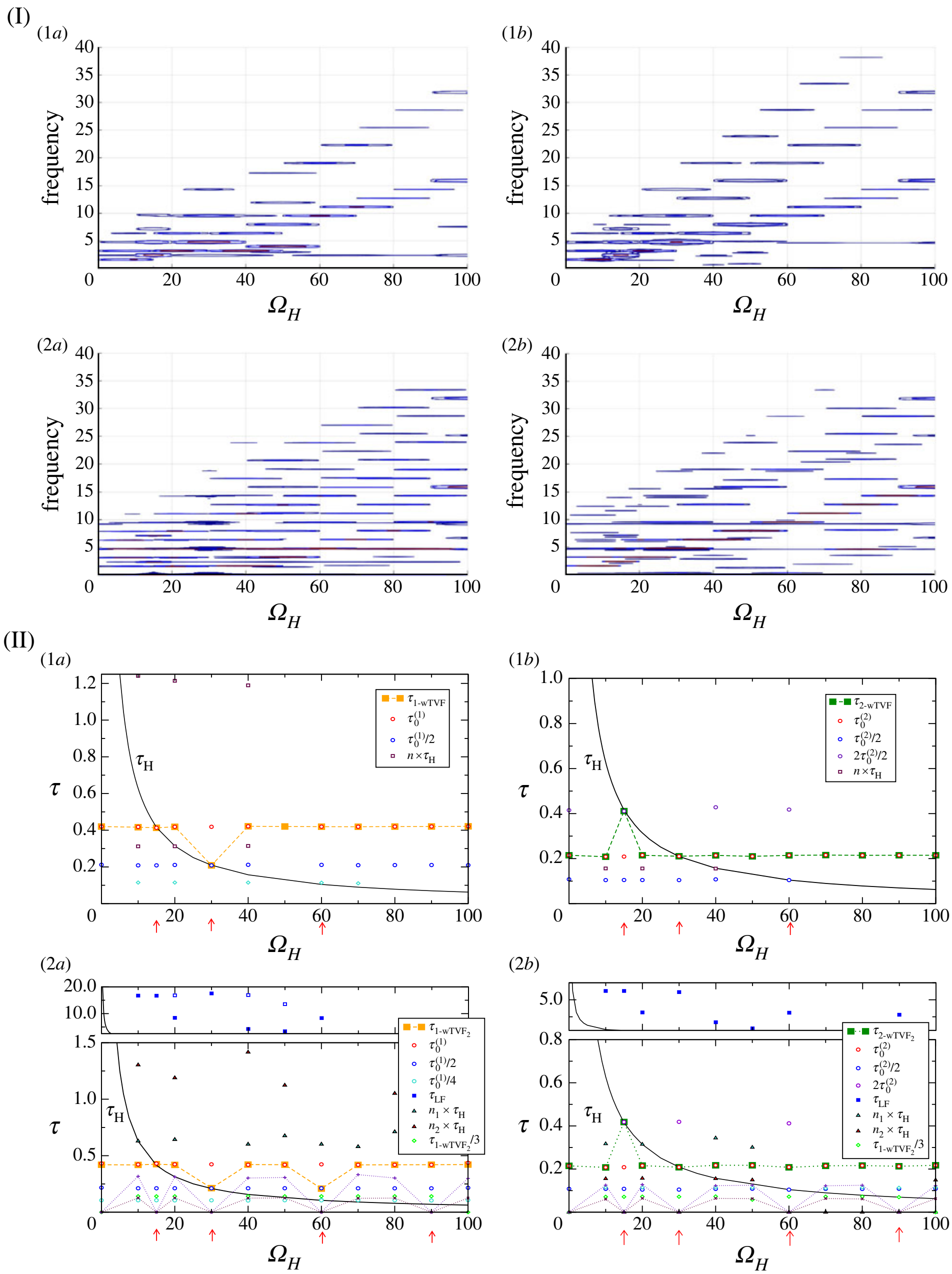

Figure 8. Frequency stimulation (I) and corresponding time periods (II) under axial (1) $s_{z,S} = 0.2$, $s_{z,M} = 0.2$ and transverse (2) $s_{x,S} = 0.2$, $s_{x,M} = 0.2$ magnetic field for (*a*) 1-wTVF$_{[2]}$ and (*b*) 2-wTVF$_{[2]}$ with variation of driving frequency Ω_H. Small arrows below the abscissa in (II) indicate the different detected resonance cases at $\Omega_H = 15, 30, 60$ for all and 90 only in the case of transverse fields. (Stars and pluses with dotted lines (only to guide the eyes) in transverse fields (2) indicate nonlinear excited modes correlated with f_{LF} which vanishes in the case of resonance. (Online version in colour.)

For 2-wTVF$_{[2]}$, the effect of variation in Ω_H is similar for oscillation under axial and transverse magnetic fields with the only former mentioned appearance of f_{LF}. The system shows resonance when stimulating with half of its natural frequency, $\Omega_H = 15 = \Omega_{2\text{-wTVF}_{[2]}}/2$, and thus, the period becomes 2-wTVF$_{[2]}$ doubled (see PD in figure 5(*b*)). Eventually, forcing with its natural frequency

$\Omega_H = 30 = \Omega_{2\text{-wTVF}_{[2]}}$ the flow dynamics become enforced. The same repeats when using twice the frequency $\Omega_H = 60 = 2 \times \Omega_{2\text{-wTVF}_{[2]}}$.

Similarly, it can be observed that for 1-wTVF$_{[2]}$, an enhancement in the dynamics when stimulated with its natural frequency $\Omega_H = 15 = \Omega_{1\text{-wTVF}_{[2]}}$. Furthermore, resonance can be seen for twice the frequency $\Omega_H = 30 = 2 \times \Omega_{1\text{-wTVF}_{[2]}}$, and so the period becomes half, similar for the axial and transverse alternating fields. However, under the transverse field, further resonance is observed when stimulating with four times its natural frequency $\Omega_H = 60 = 4 \times \Omega_{1\text{-wTVF}_{[2]}}$. Similar to the first resonance, the period becomes half (and not a quarter, as one might speculate). Nothing of this appears under axial field orientation.

(g) Flow dynamics

To get another perspective on the flow dynamics resulting from variations of the driving frequency Ω_H, in particular in the case of resonances, we focus on the azimuthal flow, which is the dominant flow in the annulus (at least for the parameters investigated here). To do so, we consider the 50% contour line of the dimensionless azimuthal velocity $v/Re = 0.50$. In addition, we use two different positions in the bulk, $\theta = 0$ (aligned with the magnetic field) and $\theta = \pi/2$ (perpendicular to the magnetic field) to account for the symmetry breaking under the transverse magnetic fields. Figure 9 (vertical grey line at $r = 1.5$ indicates the mid-gap of the bulk) illustrates these azimuthal velocity contour profiles v of 1-wTVF$_{[2]}$ and 2-wTVF$_{[2]}$, respectively, for different Ω_H.

A general observation is that the contours $v/Re = 0.50$ become more or less pronounced (that is, expanded and wider over the gap in the radial direction), which coincides with the expansion of the toroidal vortex structure of the waves. Starting with the simpler scenario of a pure axially oriented field (figure 9(1)): with increasing Ω_H (without resonances), the contours $v/Re = 0.50$ for 1-wTVF become narrower , that is, they shrink in the radial direction and minime and maxime move towards the central region (grey line at $r = 1.5$, see also insets), which means the bulges decrease. However, for the different detected resonances $\Omega_H = 15, 30$ and 60, the velocity profile of the flow without any field modulation is almost reassembled. In fact, for stimulation with its natural frequency $\Omega_H = 15$, the profile becomes even more pronounced, that is, wider (larger max and smaller min). For 2-wTVF (figure 9(1*b*)), similar profiles are observed, when stimulation occurs with the resonance frequencies $\Omega_H = 15, 30$ and 60. However, different from 1-wTVF, these do not reassemble the static scenario; the profiles are more pronounced (wider). More interesting is the fact that for even larger frequencies Ω_H, the profiles become more pronounced in general; that is, the bulges grow, which is just the opposite of the observation for 1-wTVF. As the axial field does not affect the basic system symmetries, there is a constant phase shift between $\theta = 0$ and $\theta = \pi/2$, while the profile v remains the same. Thus, for visibility only the case $\Omega_H = 0$ is shown.

In transverse field geometry, the scenario is in general more complex due to the broken symmetry with the intrinsic stimulated $m = 2$ mode. There is a large variation in profiles for $\theta = 0$ (along the applied magnetic field) and $\theta = \pi/2$ (perpendicular to the applied magnetic field). Note, in the absence of the transverse field, there is a constant phase relationship between them (cf. figure 2(*b*)). For 2-wTVF$_2$, the variation with Ω_H in the contour profiles v for $\theta = 0$ is qualitative, the same as already described for 2-wTVF in the axial field geometry with the additional variation in the phase for $\theta = \pi/2$. While the corresponding variation in contours for $\theta = \pi/2$ is qualitative, the same as for $\theta = 0$, the phase shift is not constant and varies depending on the frequency Ω_H. It is worth mentioning that the profiles for the resonance cases at $\Omega_H = 15$ and $\Omega_H = 60$ almost fall on top of each other. For 1-wTVF$_2$, a more detailed quantitative analysis is not possible due to the symmetry breaking nature of the transverse field in combination with the nonlinear interaction of the various modes present in 1-wTVF$_2$. However, the qualitative one has a similar behaviour as described for 1-wTVF in the axial field; thus, the profiles of the contours $v = Re/2$ become narrower with increasing Ω_H. Except in cases of no resonance, the profiles reassemble the natural case, and the phase shift between $\theta = 0$ and $\theta = \pi/2$ is also

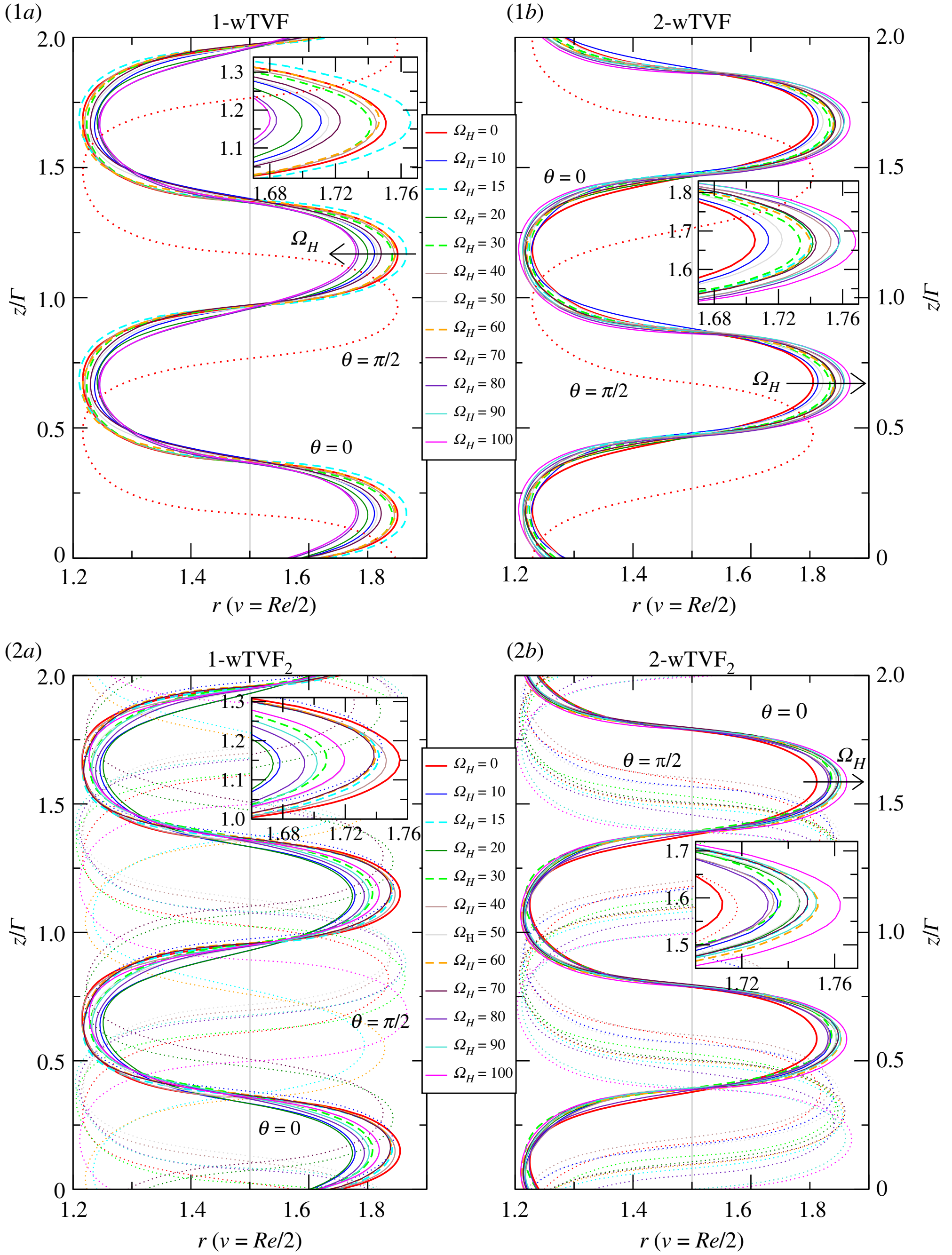

Figure 9. Azimuthal velocity contour profiles $v = Re/2$ of 1-wTVF$_{[2]}$ and 2-wTVF$_{[2]}$ in axially (1) and transverse (2) oriented magnetic field with variation of Ω_H as indicated (shown are 2Γ). The vertical grey lines at $r = 1.5$ indicate the mid-gap of the bulk. The insets show close-ups of the region where $r(v = Re/2) \approx r_{\max}$. See text for further description. Note that the angle θ has been selected to represent profiles that match at $\theta = 0$. The arrows are there to guide the eyes with increasing Ω_H (without resonances). (Online version in colour.)

more complex, that is the larger the Ω_H, the larger the differences between both azimuthal positions in the case of a transverse magnetic field. Independent of field orientation and frequency Ω_H, the centre of the contours ($v = Re/2$) always remains placed around mid-gap ($r = 1.5$) in the bulk.

5. Conclusion

Active flow control in the form of variation in the modulation frequency Ω_H of an external applied magnetic field is implemented at a fixed Reynolds number $Re = 140$ to investigate flow dynamics. The present work is focused on wavy vortex flow structures with azimuthal wavenumbers $m = 1$ and $m = 2$ in Taylor–Couette geometry with the outer cylinder at rest with the external applied and alternating magnetic field either to be axially aligned with the system symmetry axis or transversally (that is perpendicularly) to the z-symmetry axis. The latter naturally breaks the system symmetry and renders all flow structures to be inherently three-dimensional [24,25].

The flow dynamics for 1-wTVF$_{[2]}$ and 2-wTVF$_{[2]}$ are observed to undergo different resonances when forcing frequency Ω_H of the alternating magnetic fields are integer multiples or ratios of the natural frequency of the wavy vortex flows. In particular, detected resonance cases are *period doubling* and *inverse period doubling*, when stimulation of the wavy states with half or double (multiples) of their natural frequency. It is worth mentioning that these are *discrete* phenomena appearing only in the resonance case and disappearing for other frequencies.

When forcing 2-wTVF$_{[2]}$ with about half of its natural frequency ($\Omega_{2\text{-wTVF}}$) without alternating field, a first resonance appears, as the system responds with period doubling. Increasing the frequencies Ω_H expands the profiles in contours of v and therefore increases the dimension of the vortical structure (compared to the case in the absence of any magnetic field). When Ω_H is integer multiples of the natural frequency $\Omega_{2\text{-wTVF}}$, the flow dynamics are found to be almost identical; that is, the profiles v fall together, and thus, the waves have the same dynamics. At the same time, they are also stronger compared to the profiles in the absence of any magnetic field.

Forcing 1-wTVF$_{[2]}$ with about double its natural frequency ($\Omega_{1\text{-wTVF}} =$ without alternating field), the system shows resonance in the sense of inverse period doubling, as the corresponding period becomes cut in half. With increasing Ω_H the behaviour is qualitative as opposed to that seen for 2-wTVF$_{[2]}$ as the profiles v become narrower, indicating a slight compression of the vortex tubes. The latter is more clear for the axial magnetic field, while the dynamics for transverse magnetic fields are more complex and do not show such a clear tendency with increasing Ω_H. In addition, for 1-wTVF$_{[2]}$, when Ω_H is integer multiples of the natural frequency $\Omega_{1\text{-wTVF}}$, the profiles show an almost identical shape, which is, in general, different from the case in the absence of any oscillation in the magnetic field.

Furthermore, questions of interest to focus on in future studies regarding alternating magnetic fields include the analysis of wavy vortices with larger azimuthal wavenumbers as well as other more complex structures of modulated rotating waves, such as mixed ribbons, mixed-cross-spirals and many more. One particularly interesting scenario could be the analyses of wavy vortices in the parameter regime with changes between prograde and retrograde behaviour and vice-versa [22,44].

From the experimental point of view, the system configuration and parameters that were discussed in this paper are easily accessible [25]. Therefore, experiments should provide good comparison with the numerical results presented here, which are expected to be in good agreement based on the similarities between them for static magnetic fields for the onset of nonlinear instabilities. Concerning flow control, the recent experimental study of propagating vortices in axial homogeneous magnetic fields by Ilzig *et al.* [58] raises a very interesting question about what happens to these flow structures if an alternating instead of static magnetic field is applied.

Data accessibility. The datasets supporting this article are available as part of electronic supplementary material [59].

Authors' contributions. S.A.A.: conceptualization, data curation, formal analysis, investigation, methodology, visualization, writing–original draft, writing—review and editing.

Conflict of interest declaration. I declare I have no competing interests.

Funding. This work was supported by the Spanish Ministerio de Ciencia e Innovación grant no. PID2019-105162RB-I00.

Acknowledgements. S. A. is a Serra Húnter Fellow. This work has been supported by the Spanish Government under grant no. PID2019-105162RB-I00.

Appendix A

(a) Niklas function

The derived simplified ferrohydrodynamical equation of motion (3.5) provides an advantage through the effect of the magnetic field (here homogeneous but alternating with $\mathbf{H}_{z,[x]} = [H_{S,z,[x]} + H_{M,z,[x]} \sin(\Omega_{H_{z,[x]}} t)]\mathbf{e}_{z,[x]}$), and the magnetic properties of the ferrofluid on the velocity field can be characterized by a single function, the magnetic field or the (here time dependent) Niklas function [23]:

$$s_N(t)^2 = s_x(t)^2 + s_z(t)^2,$$

with

$$\begin{aligned} s_x(t) &= \sqrt{\frac{2(2+\chi)c_N}{(2+\chi)^2 - \chi^2\eta^2}} H_x = \sqrt{\frac{2(2+\chi)c_N}{(2+\chi)^2 - \chi^2\eta^2}} [H_{S,x} + H_{M,z} \sin(\Omega_{H,x} t)] \\ &= s_{S,x} + s_{M,x} \sin(\Omega_H t), \end{aligned} \tag{A 1}$$

and

$$\begin{aligned} s_z(t) &= \sqrt{c_N} H_z = \sqrt{c_N}[H_{S,z} + H_{M,z} \sin(\Omega_{H,z} t)] \\ &= s_{S,z} + s_{M,z} \sin(\Omega_H t). \end{aligned} \tag{A 2}$$

Thus, the two time-independent Niklas control parameters

$$s_{S,z[x]} = \sqrt{c_N} H_{S,z[x]} \quad \text{and} \quad s_{M,z[x]} = \sqrt{c_N} H_{M,z[x]}, \tag{A 3}$$

stand for the static contribution ($s_{S,z[x]}$) and the modulation amplitude ($s_{M,z[x]}$) of the driving, respectively.

References

1. Chossat P, Iooss G. 1994 *The Couette-Taylor problem*. Berlin, Germany: Springer.
2. Taylor GI. 1923 Stability of a viscous liquid contained between two rotating cylinders. *Phil. Trans. R. Soc. Lond. A* **223**, 289–343. (doi:10.1098/rsta.1923.0008)
3. Kuhlmann K, Roth D, Lücke M. 1989 Taylor vortex flow under harmonic modulation of the driving force. *Phys. Rev. A* **39**, 745. (doi:10.1103/PhysRevA.39.745)
4. Murray BT, McFadden GB, Coriell SR. 1990 Stabilization of Taylor–Couette flow due to time-periodic outer cylinder oscillation. *Phys. Fluids A: Fluid Dyn.* **2**, 2147. (doi:10.1063/1.857801)
5. Marques F, Lopez JM. 1997 Taylor–Couette flow with axial oscillations of the inner cylinder: Floquet analysis of the basic flow. *J. Fluid Mech.* **348**, 153–175. (doi:10.1017/S0022112097006058)
6. Normand C. 2000 Stability of time-periodic flows in a Taylor–Couette geometry. *Phys. Rotating Fluids* **549**, 67–83. (doi:10.1007/3-540-45549-3_5)
7. Marques F, Lopez J. 2000 Spacial and temporal resonances in a periodically forced hydrodynamic system. *Phys. D Nonlinear Phenom.* **136**, 340–352. (doi:10.1016/s0167-2789(99)00172-4)
8. Sinha M, Kevrekidis IG, Smiths AJ. 2006 Experimental study of a Neimark-Sacker bifurcation in axially forced Taylor–Couette flow. *J. Fluid Mech.* **558**, 1. (doi:10.1017/S0022112006009207)
9. Avila M, Marques F, Lopez JM, Meseguer A. 2007 Stability control and catastrophic transition in a forced Taylor–Couette system. *J. Fluid Mech.* **590**, 471–496. (doi:10.1017/S0022112007008105)
10. Verschoof RA, Huisman SG, Sun C, Lohse D. 2018 Periodically driven Taylor–Couette turbulence. *J. Fluid Mech.* **846**, 834–845. (doi:10.1017/jfm.2018.276)
11. Donnelly RJ. 1964 Experiments on the stability of viscous flow between rotating cylinders III. Enhancement of hydrodynamic stability by modulation. *Proc. R. Soc. Lond. A* **281**, 130–139. (doi:10.1098/rspa.1964.0173)
12. Youd AJ, Willis AP, Barenghi CF. 2005 Non-reversing modulated Taylor–Couette flows. *Fluid Dyn. Res.* **36**, 61–73. (doi:10.1016/j.fluiddyn.2004.12.001)

13. Tennakoon SGK, Andereck CD, Aouidef A, Normand C. 1997 Pulsed flow between concentric rotating cylinders. *Eur. J. Mech. B/Fluids* **16**, 227.
14. Ern P, Wesfreid JE. 1999 Flow between time-periodically co-rotating cylinders. *J. Fluid Mech.* **397**, 73–98. (doi:10.1017/S0022112099006059)
15. Gassa Feugaing CM, Crumeyrolle O, Yang KS, Mutabazi I. 2014 Destabilization of the Couette Taylor flow by modulation of the inner cylinder rotation. *Eur. J. Mech.-B/Fluids* **44**, 82–87. (doi:10.1016/j.euromechflu.2013.10.006)
16. Rosensweig RE. 1985 *Ferrohydrodynamics*. Cambridge, UK: Cambridge University Press.
17. Altmeyer S. 2020 Ferrofluids. *Scholarpedia* **15**, 55163. (doi:10.4249/scholarpedia.55163)
18. McTague JP. 1969 Magnetoviscosity of magnetic colloids. *Chem. Phys.* **51**, 133–136. (doi:10.1063/1.1671697)
19. Rosensweig RE, Kaiser R, Miskolczy G. 1969 Magnetoviscosity of magnetic fluid in a magnetic field. *J. Colloid Interface Sci.* **29**, 680. (doi:10.1016/0021-9797(69)90220-3)
20. Berkovsky B, Bashtovoy V. 1996 *Magnetic fluids and applications handbook*. New York, NY: Begel House.
21. Blums E, Cebers A, Maiorov MM. 1997 *Magnetic fluids*. Berlin, Germany: Walter de Gruyter.
22. Altmeyer S, Do Y, Lai Y-C. 2015 Magnetic field induced flow pattern reversal in a ferrofluidic Taylor–Couette system. *Sci. Rep.* **5**, 18589. (doi:10.1038/srep18589)
23. Niklas M. 1987 Influence of magnetic fields on Taylor vortex formation in magnetic fluids. *Z. Phys. B* **68**, 493–501. (doi:10.1007/BF01471080)
24. Altmeyer S, Hoffmann C, Leschhorn A, Lücke M. 2010 Influence of homogeneous magnetic fields on the flow of a ferrofluid in the Taylor–Couette system. *Phys. Rev. E* **82**, 016321. (doi:10.1103/PhysRevE.82.016321)
25. Reindl M, Odenbach S. 2011 Effect of axial and transverse magnetic fields on the flow behavior of ferrofluids featuring different levels of interparticle interaction. *Phys. Fluids* **23**, 093102. (doi:10.1063/1.3633341)
26. Singh J, Bajaj R. 2005 Couette flow in ferrofluids with magnetic field. *J. Magn. Magn. Matter.* **294**, 53–62. (doi:10.1016/j.jmmm.2004.10.123)
27. Niklas M, Müller-Krumbhaar H, Lücke M. 1989 Taylor–vortex flow of ferrofluids in the presence of general magnetic fields. *J. Magn. Magn. Mater.* **81**, 29–38. (doi:10.1016/0304-8853(89)90225-4)
28. Singh J, Bajaj R. 2008 Parametric modulation in the Taylor–Couette ferrofluid flow. *Fluid Dyn. Res.* **40**, 737–752. (doi:10.1016/j.fluiddyn.2008.04.002)
29. Altmeyer S, Lopez J, Do Y. 2012 Influence of an inhomogeneous internal magnetic field on the flow dynamics of ferrofluid between differentially rotating cylinders. *Phys. Rev. E* **85**, 066314. (doi:10.1103/PhysRevE.85.066314)
30. Wereley ST, Lueptow RM. 1998 Spatio-temporal character of non-wavy and wavy Taylor–Couette flow. *J. Fluid Mech.* **364**, 59–80. (doi:10.1017/s0022112098008969)
31. Akonur A, Lueptow RM. 2003 Three-dimensional velocity field for wavy Taylor–Couette flow. *Phys. Fluids* **15**, 947–960. (doi:10.1063/1.1556615)
32. Andereck CD, Liu SS, Swinney HL. 1986 Flow regimes in a circular Couette system with independently rotating cylinders. *J. Fluid Mech.* **164**, 155–183. (doi:10.1017/s0022112086002513)
33. Gollub JP, Swinney HL. 1975 *Hydrodynamic instabilities and the transition to turbulence*. Berlin, Germany: Springer.
34. Egbers C, Pfister G. 2000 *Physics of rotating fluids*. Berlin, Germany: Springer.
35. Gill A. 1982 *Atmosphere-ocean dynamics*. San Diego, CA: Academic Press.
36. Davey A, Di Prima RC, Stuart JT. 1968 On the instability of Taylor vortices. *J. Fluid Mech.* **31**, 17. (doi:10.1017/S0022112068000029)
37. Iooss G. 1986 Secondary bifurcations of Taylor vortices into wavy inflow or outflow boundaries. *J. Fluid Mech.* **173**, 273–288. (doi:10.1017/S0022112086001179)
38. Altmeyer S, Do Y, Marques F, Lopez JM. 2012 Symmetry-breaking Hopf bifurcations to 1-, 2-, and 3-tori in small-aspect-ratio counterrotating Taylor–Couette flow. *Phys. Rev. E* **86**, 046316. (doi:10.1103/PhysRevE.86.046316)
39. Coles D. 1965 Transition in circular Couette flow. *J. Fluid Mech.* **21**, 385–425. (doi:10.1017/S0022112065000241)
40. Jones CA. 1981 Nonlinear Taylor vortices and their stability. *J. Fluid Mech.* **102**, 249–261. (doi:10.1017/S0022112081002620)

41. Hoffmann C, Altmeyer S, Pinter A, Lücke M. 2009 Transitions between Taylor vortices and spirals via wavy Taylor vortices and wavy spirals. *New J. Phys.* **11**, 053002. (doi:10.1088/1367-2630/11/5/053002)
42. Ahlers G, Cannell DS, Dominguez-Lerma MA. 1983 Possible mechanism for transitions in wavy Taylor-vortex flow. *Phys. Rev. A* **27**, 1225–1227. (doi:10.1103/PhysRevA.27.1225)
43. Marcus PS. 1984 Simulation of Taylor–Couette flow. Part 2. Numerical results for wavy-vortex flow with one travelling wave. *J. Fluid Mech.* **146**, 65–113. (doi:10.1017/S0022112084001774)
44. Altmeyer S, Lueptow R. 2017 Wave propagation reversal for wavy vortices in wide-gap counter-rotating cylindrical Couette flow. *Phys. Rev. E* **95**, 053103. (doi:10.1103/PhysRevE.95.053103)
45. Altmeyer S, Do Y, Lai Y-C. 2015 Transition to turbulence in Taylor–Couette ferrofluidic flow. *Sci. Rep.* **5**, 10781. (doi:10.1038/srep10781)
46. Altmeyer S. 2021 Propagating vortices in ferrofluidic Couette flow under magnetic fields - part I: axial and symmetry breaking transversal oriented fields. *J. Magn. Magn. Mater.* **527**, 167769. (doi:10.1016/j.jmmm.2021.167769)
47. Altmeyer S. 2021 Propagating vortices in ferrofluidic Couette flow under magnetic fields - part II: oblique oriented fields. *J. Magn. Magn. Mater.* **527**, 167788. (doi:10.1016/j.jmmm.2021.167788)
48. Altmeyer S. 2021 On the ridge of instability in ferrofluidic Couette flow via alternating magnetic field. *Sci. Rep.* **11**, 4705. (doi:10.1038/s41598-021-84175-z)
49. Altmeyer S. 2022 Increasing flow complexity in time-dependent modulated ferrofluidic couette flow. *Fluid Dyn.* **57**, 387–400. (doi:10.1134/S0015462822030016)
50. Müller HW, Liu M. 2001 Structure of ferrofluid dynamics. *Phys. Rev. E* **64**, 061405. (doi:10.1103/physreve.64.061405)
51. Altmeyer S, Lopez J, Do Y. 2013 Effect of elongational flow on ferrofuids under a magnetic field. *Phys. Rev. E* **88**, 013003. (doi:10.1103/PhysRevE.88.013003)
52. Langevin P. 1905 Magnétisme et théorie des électrons. *Annales de Chemie et de Physique* **5**, 70.
53. Embs J, Müller HW, Wagner C, Knorr K, Lücke M. 2000 Measuring the rotational viscosity of ferrofluids without shear flow. *Phys. Rev. E* **61**, R2196–R2199. (doi:10.1103/PhysRevE.61.R2196)
54. Odenbach S, Müller HW. 2002 Stationary off-equilibrium magnetization in ferrofluids under rotational and elongational flow. *Phys. Rev. Lett.* **89**, 037202. (doi:10.1103/PhysRevLett.89.037202)
55. Altmeyer S. 2022 Ferrofluidic Couette flow in time-varying magnetic field. *J. Magn. Magn. Mater.* **552**, 169205. (doi:10.1016/j.jmmm.2022.169205)
56. Hana X, Chen Z, Bi Q. 2016 Inverse period-doubling bifurcations determine complex structure of bursting in a one-dimensional non-autonomous map. *Chaos* **26**, 023117. (doi:10.1063/1.4942503)
57. Sarwar W, Mellibovsky F, Alam M.M, Zafar F. 2021 Transition to periodic behaviour of flow past a circular cylinder under the action of fluidic actuation in the transitional regime. *Energies* **14**, 5069. (doi:10.3390/en14165069)
58. Ilzig T, Stöckel K, Odenbach S. 2019 Experimental investigations on the effect of axial homogenous magnetic fields on propagating vortex flow in the Taylor–Couette System. *Materials* **12**, 4027. (doi:10.3390/ma12244027)
59. Altmeyer SA. 2023 Ferrofluidic wavy Taylor vortices under alternating magnetic field. Figshare. (doi:10.6084/m9.figshare.c.6350552)